BIOCHEMISTRY
including biophysical chemistry & molecular biology
Article

Biochemistry **2009,** *48,* 11011–11025 11011
DOI: 10.1021/bi901069h

The Thiolase Reaction Mechanism: The Importance of Asn316 and His348 for Stabilizing the Enolate Intermediate of the Claisen Condensation[†]

Gitte Meriläinen,[§,∥,⊥] Visa Poikela,[§,∥,⊥] Petri Kursula,[§] and Rik K. Wierenga*[,§,∥]

[§]*Department of Biochemistry, University of Oulu, P.O. Box 3000, 90014 Oulu, Finland, and* [∥]*Biocenter Oulu, University of Oulu, P.O. Box 5000, 90014 Oulu, Finland.* [⊥]*These authors contributed equally to these studies.*

Received June 24, 2009; Revised Manuscript Received September 21, 2009

ABSTRACT: The biosynthetic thiolase catalyzes a Claisen condensation reaction between acetyl-CoA and the enzyme acetylated at Cys89. Two oxyanion holes facilitate this catalysis: oxyanion hole I stabilizes the enolate intermediate generated from acetyl-CoA, whereas oxyanion hole II stabilizes the tetrahedral intermediate of the acetylated enzyme. The latter intermediate is formed when the α-carbanion of acetyl-CoA enolate reacts with the carbonyl carbon of acetyl-Cys89, after which C−C bond formation is completed. Oxyanion hole II is made of two main chain peptide NH groups, whereas oxyanion hole I is formed by a water molecule (Wat82) and NE2(His348). Wat82 is anchored in the active site by an optimal set of hydrogen bonding interactions, including a hydrogen bond to ND2(Asn316). Here, the importance of Asn316 and His348 for catalysis has been studied; in particular, the properties of the N316D, N316A, N316H, H348A, and H348N variants have been determined. For the N316D variant, no activity could be detected. For each of the remaining variants, the k_{cat}/K_m value for the Claisen condensation catalysis is reduced by a factor of several hundred, whereas the thiolytic degradation catalysis is much less affected. The crystal structures of the variants show that the structural changes in the active site are minimal. Our studies confirm that oxyanion hole I is critically important for the condensation catalysis. Removing either one of the hydrogen bond donors causes the loss of at least 3.4 kcal/mol of transition state stabilization. It appears that in the thiolytic degradation direction, oxyanion hole I is not involved in stabilizing the transition state of its rate limiting step. However, His348 has a dual role in the catalytic cycle, contributing to oxyanion hole I and activating Cys89. The analysis of the hydrogen bonding interactions in the very polar catalytic cavity shows the importance of two conserved water molecules, Wat82 and Wat49, for the formation of oxyanion hole I and for influencing the reactivity of the catalytic base, Cys378, respectively. Cys89, Asn316, and His348 form the CNH-catalytic triad of the thiolase superfamily. Our findings are also discussed in the context of the importance of this triad for the catalytic mechanism of other enzymes of the thiolase superfamily.

The Claisen condensation reaction, by which a C−C bond is formed, is an important reaction in the living world (*1*). In this reaction, a nucleophilic carbanion is generated in the active site of the enzyme. In the enzymatic conversion that is considered here, this concerns the α-carbon of a thioester moiety, and the activation is achieved in one of two ways, by either decarboxylation or deprotonation (*2*). The thioester moiety is a fragment of a pantetheine-acyl molecule, which is part of either acyl-CoA[1] or acyl-ACP (acyl carrier protein). The activation by decarboxylation is important, for example, in fatty acid synthesis, in which case the substrate malonyl-ACP is activated by decarboxylation in the active sites of 3-ketoacyl-CoA-ACP-synthases (KAS enzymes). The activated α-methyl group of acetyl-ACP subsequently performs a nucleophilic attack on the carbonyl carbon atom of the acylated enzyme, and in this reaction, a C−C bond is formed. In other enzymes, including thiolases, the bound acetyl-CoA is activated by deprotonation by a nearby base. Thiolases and KAS enzymes have the same fold and both belong to the thiolase superfamily, which also includes the polyketide synthases (PKS) and chalcone synthases (CHS) (*3*). Enzymes that belong to the thiolase superfamily can be grouped into two main groups, the nondecarboxylating (including the thiolase subfamily) and the decarboxylating subgroup (such as the KAS enzymes) (*4*). The overall thiolase fold and the catalytic cysteine, which is covalently acylated during the reaction cycle, are preserved in the superfamily, and the smallest common structural unit is a dimer.

Thiolases are ubiquitous enzymes, essential in a range of metabolic pathways. They occur as dimers or tetramers, which are dimers of dimers. In humans, six different thiolases have been described, located in the cytosol (the CT thiolase), in peroxisomes (the A/B-thiolase and the SCP2-thiolase), and in mitochondria (the T1 thiolase, the T2 thiolase, and the thiolase subunit of the α4β4-trifunctional enzyme, TFE). The peroxisomal thiolases are dimers, whereas the CT, T1, and T2 thiolases are tetrameric. All of these enzymes have a clear sequence similarity with each other, indicating a common evolutionary history (*5*). Each thiolase subunit consists of approximately 400 residues and folds into three domains: the N- and C-terminal core domains and a loop domain, which protrudes out of the N-terminal domain and covers the active site. The N- and C-terminal core domains have identical topology, with a mixed β-sheet covered by helices. The

[†]This research has been supported by grant 1122921 from the Academy of Finland.

* To whom correspondence should be addressed. Phone: +358-8-5531199. Fax: +358-8-5531141. E-mail: Rik.Wierenga@oulu.fi.

[1]Abbreviations: CoA, coenzyme A; Ac-CoA, acetyl-CoA; AcAc-CoA, acetoacetyl-CoA.

© 2009 American Chemical Society
Published on Web 10/20/2009

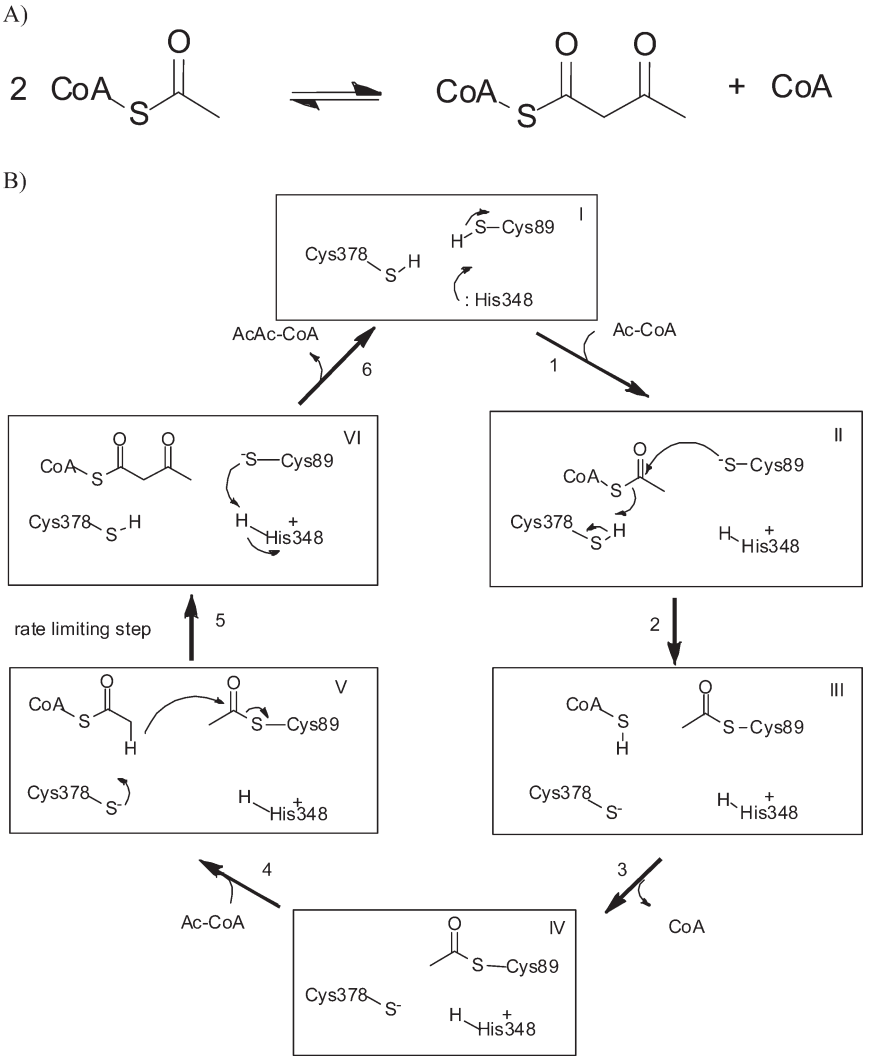

FIGURE 1: Reaction of thiolase. (A) The overall reaction of thiolase in the synthetic direction. The equilibrium of the reaction favors the reverse thiolytic direction. (B) The catalytic cycle of thiolase (*7*). The arrows visualize the catalytic cycle in the condensation direction. The rate limiting step is the Claisen condensation reaction (step 5), in which the acetyl group is transferred from Cys89 (in complex V) to acetyl-CoA, by which acetoacetyl-CoA (complex VI) is formed. Cys89 is activated by His348; Cys378 is activated by waters Wat82 and Wat49. This is a simplified diagram and not all possibly relevant protonation/deprotonation steps are included.

two core domains assemble into a compact 5-layered $\alpha\beta\alpha\beta\alpha$ sandwich fold. The central helical layer is formed by the two buried catalytic helices, Nα3 and Cα3, of the N- and C-terminal core domains, respectively.

The thiolase isoenzymes have different substrate specificities, different catalytic efficiencies, and different cellular functions. Thiolases catalyze the synthetic reaction (Figure 1) as well as its reverse degradative reaction, but the equilibrium is in favor of thiolysis. Thiolases functioning in degradative pathways convert 3-ketoacyl-CoA molecules into acetyl-CoA and acyl-CoA, whereas biosynthetic thiolases catalyze the synthesis of acetoacetyl-CoA from two molecules of acetyl-CoA (Figure 1). The peroxisomal thiolases are degradative thiolases involved in fatty acid degradation (the A/B thiolase) and bile acid synthesis (the SCP2 thiolase). The mitochondrial thiolases are involved in fatty acid degradation (the T1 and $\alpha4\beta4$ thiolases) as well as ketone body synthesis and ketone body degradation (the T2 thiolase). The human cytosolic thiolase (CT) is a key enzyme in the synthesis pathway of steroid molecules; it is a close homologue of the bacterial *Zoogloea ramigera* biosynthetic thiolase, which is known to be one of the most efficient thiolases. The *Z. ramigera* thiolase is also the best characterized thiolase (*6*−*8*); it functions in a pathway for the synthesis of a polyester, polyhydroxybuturate, which acts as an intracellular energy reserve (*9*, *10*). The studies reported here have been done with the *Z. ramigera* thiolase.

Figure 1B visualizes the complete catalytic cycle of thiolase in the synthetic direction, resulting in the synthesis of acetoacetyl-CoA from two molecules of acetyl-CoA. In the context of this study, the Claisen condensation reaction specifically refers to the reaction 5 (clockwise) of Figure 1B. In the thiolytic direction, 3-ketoacyl-CoA molecules are degraded by proceeding counterclockwise in the diagram of Figure 1B. All thiolases catalyze both reactions. Except when mentioned otherwise, the reaction mechanistic discussions in this study concern the synthetic direction. In the C−C bond forming reaction, the nucleophilic α-carbanion of acetyl-CoA attacks the electrophilic carbonyl carbon of the acetylated cysteine, and a new carbon−carbon bond is formed. Two intermediates, a tetrahedral and an enolate intermediate (Figure 2) are important in this conversion. In thiolases, the nucleophilic α-carbon is always formed by proton abstraction by a catalytic base (Figure 1). For the *Z. ramigera* thiolase, several structures are available of trapped intermediate complexes of the reaction cycle. The four key catalytic residues are Cys89, Asn316,

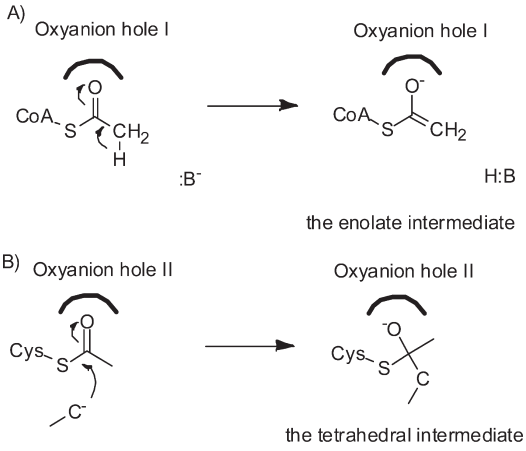

FIGURE 2: Enolate and tetrahedral intermediates of the Claisen condensation reaction. (A) Abstraction of the acetyl-CoA α-methyl proton by a base (Cys378) generates the enolate intermediate, which is stabilized by oxyanion hole I. (B) Nucleophilic attack by the acetyl-CoA α-methyl carbanion on the Cys89-thioester carbonyl carbon generates the tetrahedral oxyanion, which is stabilized by oxyanion hole II.

His348, and Cys378. Cys89 provides the nucleophilic group, which becomes acetylated in the first step of the reaction (*1*). The crystal structures suggest that NE2(His348) deprotonates Cys89, activating it for this acyl transfer reaction. The side chain of His348 is fixed in its position by a hydrogen bond between ND1(His348) and OG(Ser353) (Figure 3). In the acylated form, the Cys89 side chain is rotated toward NE2(His348), which is predicted to remain positively charged throughout the catalytic cycle. Upon acylation of Cys89, it has been proposed that Cys378 becomes negatively charged after donating its proton to the leaving group of the acetylation reaction, CoA (complex III, Figure 1B) (*7*). Subsequently, Cys378 is the catalytic base, deprotonating the C2 carbon of acetyl-CoA in the second half of the synthetic reaction, resulting in the formation of an enolate intermediate (Figure 2). The crystal structures of the intermediates show that the active site is very rigid, without flexible loops, and the only structural changes of the protein concern the small side chain rotation of Cys89 when comparing the structure of the apo enzyme with the various liganded structures (Figure 3). In all liganded structures, including CoA, acetyl-CoA, and acetoacetyl-CoA, the mode of binding of CoA is preserved, and in each complex, the CoA sulfur atom is bound in the same position.

The four catalytic residues protrude out of four catalytic loops (*8*). Cys89 is in a loop at the N-terminus of helix Nα3; Asn316, His348, and Cys378 are in the C-terminal core domain. Asn316 is in the Cβ2-Cα2 loop, His348 in the Cβ3-Cα3 loop, and Cys378 in the Cβ4-Cβ5 loop. The spatial geometry of these four catalytic residues is shown in Figure 3. In the crystal structures, His348 is interacting with both Cys89 and Asn316. The SG-(Cys89)-NE2(His348) distance is 3.1 Å and the CE1(His348)-ND2(Asn316) distance is 3.4 Å. An important feature of the active site is the presence of two oxyanion holes. As shown in Figure 3, Asn316 and His348 are important for the geometry of oxyanion hole I. The two components of this oxyanion hole are a water molecule, Wat82, stabilized by the Asn316 side chain, and NE2(His348). His348, therefore, appears to have two catalytic functions, being involved in the activation of Cys89 and in the formation of oxyanion hole I. Oxyanion hole II is formed by the main chain NH groups of Cys89 and Gly380. Oxyanion hole I binds the thioester oxygen atom of the substrates acetyl-CoA (in the synthetic direction) and acetoacetyl-CoA (in the degradative direction). The binding of the thioester oxygen of acetyl-CoA in oxyanion hole I predicts that oxyanion hole I is of particular importance for the Claisen condensation chemistry. Oxyanion hole II binds the thioester oxygen of acetyl-Cys89, as well as the 3-keto oxygen of acetoacetyl-CoA (*7*). Oxyanion hole II will thus facilitate the thiolytic cleavage of acetoacetyl-CoA as well as the Claisen condensation reaction, in both cases stabilizing the negatively charged oxyanion of a tetrahedral intermediate (Figure 2). For oxyanion hole I, the Wat82-Asn316 diad is one of the hydrogen bonding partners. Wat82 is part of a hydrogen bonding network, extending via Wat49 and a trail of waters toward the back side of the molecule (Figure 3B).

In the thiolase superfamily, the residues corresponding to Asn316 and His348 of *Z. ramigera* thiolase are highly conserved: only a histidine or asparagine is observed in these positions (*8*). Jiang et al. (*4*) have subdivided the thiolase superfamily into three categories: CHH, CNH, and CHN. The C refers to the conserved catalytic cysteine (Cys89), conserved throughout the superfamily. In the thiolase subfamily, the combination of an asparagine (at position 316, the proximal residue) and a histidine (at position 348, the distal residue) is mostly conserved (CNH category), except in some thiolases in which a His-His pair is observed (CHH category) (*4*). All known thiolases can, therefore, be classified as either CNH or CHH. Other members of the superfamily, such as the KAS enzymes, belong to either the CHH or the CHN family. None of superfamily members has a CNN motif (*4*).

The full conservation of the C(H/N,H/N)-motifs is an intriguing observation. Several catalytic functions have been proposed for these active-site histidines and asparagines, but for most enzymes, there are no structures available of a competent ternary complex. For the KAS enzymes, it has been proposed that the proximal histidine is involved in the decarboxylation step, either (i) by activating a nucleophilic water or (ii) by stabilizing the intermediate as a hydrogen bond donor in the oxyanion hole for the enolate intermediate (*11*). The latter proposal agrees with the insight of the thiolase reaction, for which the structure of a competent ternary complex is available. The structure of this complex of acetyl-CoA bound to the acetylated enzyme visualizes the active site geometry required to catalyze the Claisen condensation (PDB entry 1DM3 (*12*)). In this complex, the thioester oxygen of acetyl-CoA interacts with the Asn316/Wat82 dyad and NE2(His348), and this geometry has identified oxyanion hole I, as highlighted in Figure 3.

To understand better the intriguing conservation of these asparagines and histidines within the superfamily, Asn316 and His348 of *Z. ramigera* thiolase were mutated and the properties of the variants were carefully evaluated using enzyme kinetic measurements, biophysical approaches, and X-ray crystallography. These studies were also aimed at quantifying the role of Asn316 and His348 and, thus oxyanion hole I, for the transition state stabilization in the catalytic cycle of the bacterial thiolase.

From the classical studies on serine proteases and esterases, it has been established that oxyanion holes are very important tools of active site geometries for catalyzing reactions in which a negatively charged tetrahedral oxyanion is a key feature of the reaction cycle (*13*−*15*). In cutinase, which is also an esterase, the donors are two main chain NH groups and a serine side chain. The removal of the serine side chain hydrogen bond donor reduces the rate by a factor of approximately 2000, while the

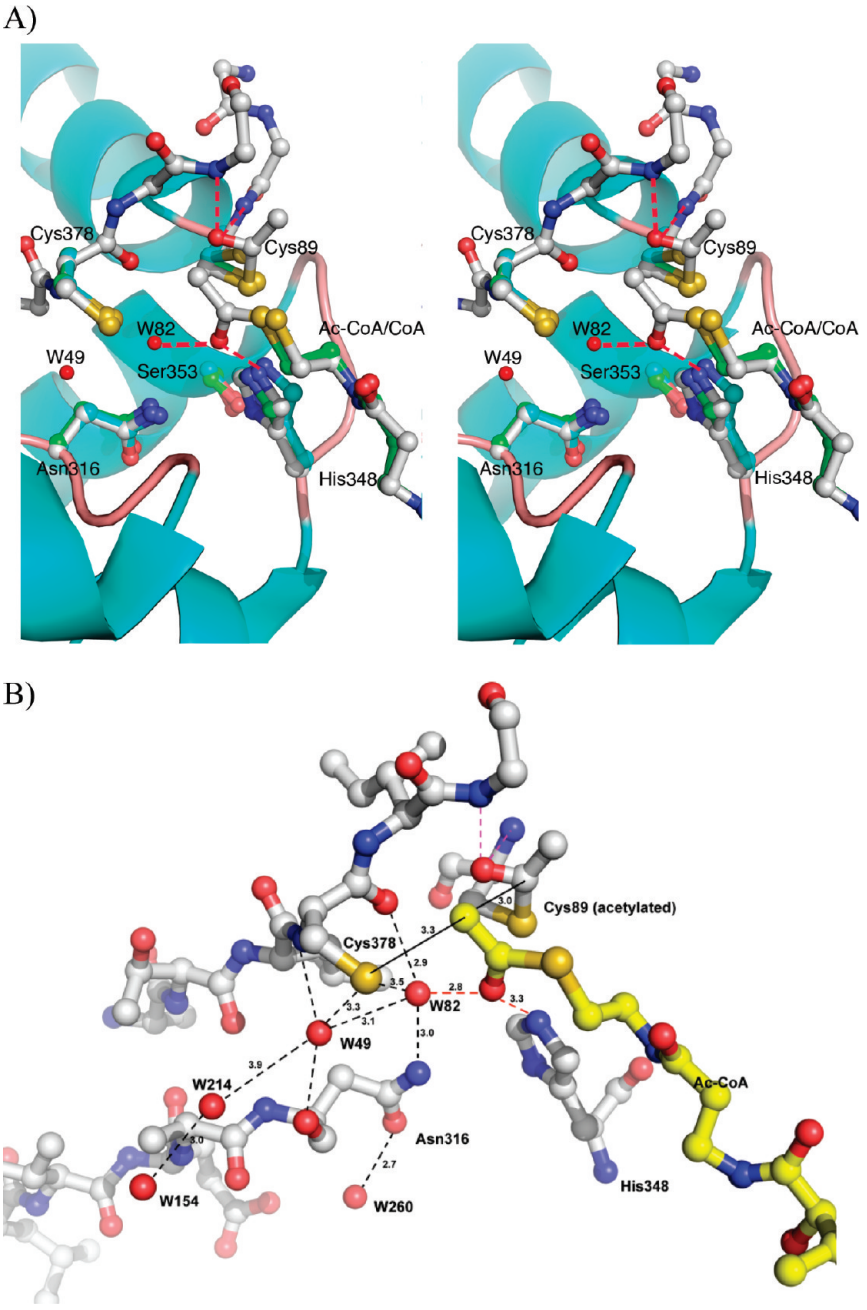

FIGURE 3: Wild type thiolase active site geometry. (A) The active site geometry of the acetylated enzyme, complexed with acetyl-CoA (1DM3, green), is visualized. Also shown are the CoA molecule of the CoA-complexed structure (1DLV, gray), bound in the same way as in the acetylated complex, as well as the apo structure (1DLU, cyan). His348 is anchored via a hydrogen bond between ND1(His348) and OG(Ser353). The red dashed lines highlight oxyanion hole I (near the acetyl-CoA thioester moiety) and oxyanion hole II (near the Ac-Cys89 thioester moiety). Cys89 and Ser353 are at the N termini of the buried catalytic helices, Nα3 and Cα3, respectively. (B) The trail of waters extending from Wat82 and Wat49. The Cys378 side chain is buried in this complex (1DM3). The red dashed lines highlight the oxyanion holes. Wat260 is part of a buried water cluster, as described previously (*7*).

crystal structure shows that there are no structural rearrangements other than the serine to alanine mutation (*16*). In some other serine proteases and esterases, for example, in subtilisin (*17*), papain (*18*), and lipase (*19*), also a side chain is one of the hydrogen bond donors, providing either an NH- or an OH-group. Mutagenesis of these side chain hydrogen bond donors also reduces the catalytic rate approximately 1000-fold, but in these cases, there are no corresponding crystal structures available. In each of these studies, it was found that the affinity for substrate remains relatively unaffected. Following the treatment developed by Fersht (*20*, *21*), it has been calculated from the cutinase data that the transition state stabilization of one hydrogen bond donor of the oxyanion hole is 3.3 kcal/mol. This is the loss of transition state stabilization free energy, $\Delta\Delta G^{\ddagger}$, which can be calculated from the kinetic constants k_{cat} and K_m, more specifically from the k_{cat}/K_m ratio:

$$\Delta\Delta G^{\ddagger} = -RT \ln \frac{(k_{cat}/K_m)\text{mutant}}{(k_{cat}/K_m)\text{wildtype}}$$

The two oxyanion holes of thiolase have rather different properties and belong to different classes. Oxyanion hole II (Figure 3) is of the same category as the classical oxyanion hole, as found in serine proteases and esterases: it is formed by two

main chain peptide NH groups, and it binds a tetrahedral intermediate (Figure 2). Oxyanion hole I of thiolase, stabilizing the enolate intermediate, is unique, because a water molecule is one of the hydrogen bonding partners. Oxyanion holes, in which a water molecule is a hydrogen bonding partner, are not very well characterized. A recent survey of active sites with oxyanion holes (*22*), however, shows that such oxyanion holes do occur frequently in CoA-dependent enolizing enzymes. Well known examples include citrate synthase (*23*) and enzymes of the crotonase superfamily (*24*). In these enolizing enzymes, like in thiolase, an enolate intermediate is also formed after the abstraction of a proton from a carbon adjacent to a thioester moiety. The enolate intermediate is distinctly different from a tetrahedral oxyanion intermediate. In the formation of the tetrahedral intermediate, the oxyanion moves out of the plane of the carbonyl moiety (*25*), whereas upon formation of the enolate from the carbonyl moiety, no atomic rearrangements of the thioester moiety need to be invoked (Figure 2).

Oxyanion hole I, formed by the Asn316-Wat82 dyad and His348, is predicted to be critically important for the condensation reaction, which is initiated by proton abstraction from acetyl-CoA by Cys378. The enolate intermediate, formed after this proton abstraction, is stabilized by oxyanion hole I. The studies reported here show that oxyanion hole I is not important for the affinity of the substrate but, rather, for stabilizing the enolate transition state. The importance of the electrostatic properties and hydrogen bonding interactions in the thiolase active site for the thiolase reaction mechanism are also discussed.

EXPERIMENTAL PROCEDURES

Site-Directed Mutagenesis of Bacterial Thiolase. The thiolase variants N316A, N316H, N316D, H348A, H348N, and N316H−H348N were created with the QuikChange site-directed mutagenesis kit (Stratagene) using the plasmid pTrc99A::thiolase, encoding for wild type *Z. ramigera* thiolase (*26*) as a template. The primers for mutagenesis (TAG, Copenhagen, Denmark), for sense and antisense directions, were designed with the QuikChange primer design program (Stratagene). The presence of the desired mutation was confirmed by sequencing.

Expression and Purification of Bacterial Thiolase and Its Variants. The wild type and mutated thiolases were expressed in the *E. coli* BL21(DE3)-pLysS strain. The expression and purification protocols were as previously described (*26*), with the exception that the mutated variants were induced with 0.4 mM IPTG at 20 °C overnight instead of 37 °C for the wild type. This was done to overcome possible problems in folding of the mutated proteins. Purified protein was stored at −20 °C in a buffer containing 5 mM Tris-HCl (pH 8.1), 1 mM EDTA, 0.5 mM DTT, 50% glycerol, and 10 mM β-mercaptoethanol. Protein concentrations were determined by measuring the absorbance at a wavelength of 280 nm.

Expression and Purification of Recombinant Human Short-Chain L-3-Hydroxyacyl-CoA Dehydrogenase. Plasmid pET28a::SCHAD encoding for human recombinant short-chain L-3-hydroxyacyl-CoA dehydrogenase (SCHAD) (*27*) was transformed into BL21(DE3)pLysS strain. Cells were cultured in M9ZB media supplemented with 30 μg/mL kanamycin and 34 μg/mL chloramphenicol. Induction with IPTG was done as described previously (*28*). After induction, cells were harvested by centrifugation, washed with 1× PBS buffer and stored at −70 °C.

For purification, cells were thawed and suspended in 0.1 M sodium phosphate buffer (pH 7.8) containing 300 mM NaCl. Cell lysis was ensured by adding 100 μg/mL lysozyme. DNA and RNA were degraded by the addition of 25 μg/mL DNase I and RNase A and 5 mM $MgCl_2$. The suspension was incubated at room temperature for 20 min, after which the cell debris were removed by centrifugation (30000*g*, 45 min at +4 °C). Purification of SCHAD was performed as described previously (*28*). Enzyme activity was measured using the Mg^{2+} method (*29*, *30*). The purified protein was stored at +4 °C in 0.1 M sodium phosphate buffer (pH 7.8) containing 300 mM NaCl.

Crystallization. For all crystallization experiments, the protein was prepared in a buffer containing 10 mM Tris-HCl (pH 8.1), 1 mM EDTA, 1 mM DTT, 5% glycerol, and 10 mM β-mercaptoethanol, at a concentration range of 1.0−2.5 mg/mL. Crystallization was done at 22 °C using the hanging drop method. In the case of cocrystallization experiments with CoA, the protein solution contained 4 mM CoA. Unless otherwise mentioned, the drops were prepared by mixing 2 μL of protein with 2 μL of the well solution.

For growing the N316A crystals, the well solution contained 1.9 M $(NH_4)_2SO_4$, 0.1 M sodium citrate (pH 6.5), 1 mM EDTA, 1 mM NaN_3, and 1 mM DTT. The protein solution (2 mg/mL) contained also 4 mM CoA.

The N316H crystals were obtained in the absence of CoA, in hanging drops equilibrated with 0.95 M Li_2SO_4, 1.3 M $(NH_4)_2SO_4$, 0.1 M sodium citrate (pH 5.5), 1 mM EDTA, 1 mM NaN_3 and 1 mM DTT. The protein concentration in the protein solution was 2 mg/mL.

N316D was crystallized using 1.9 M $(NH_4)_2SO_4$, 0.1 M 2-(*N*-morpholino)ethanesulfonic acid (MES) (pH 5.7), 1 mM EDTA, 1 mM NaN_3, and 1 mM DTT in hanging drops (1 + 1 μL). The protein concentration in the protein solution was 1 mg/mL, and 4 mM CoA was also present.

Crystals of the H348A variant were eventually obtained by microseeding. The protein was mixed with the well solution (0.95 M Li_2SO_4, 1.2 M $(NH_4)_2SO_4$, 0.1 M sodium citrate (pH 5.5), 1 mM EDTA, 1 mM NaN_3, and 1 mM DTT) and equilibrated with the hanging drop vapor diffusion method for two days at 22 °C. The resulting small crystals were smashed into pieces and used for microseeding. This time, the protein solution (1.5 mg/mL) contained 4 mM CoA, and it was mixed with well solution (2 + 2 μL) consisting of 0.95 M Li_2SO_4, 1.1 M $(NH_4)_2SO_4$, 0.1 M sodium citrate (pH 5.5), 1 mM EDTA, 1 mM NaN_3, and 1 mM DTT.

The variant H348N was cocrystallized using a well solution containing 0.75 M Li_2SO_4, 1.7 M $(NH_4)_2SO_4$, 0.1 M sodium citrate (pH 5.5), 1 mM EDTA, 1 mM NaN_3, and 1 mM DTT. The protein concentration in the protein solution was 1.5 mg/mL, and 4 mM CoA was also present. Crystals grew in two weeks.

The variant N316H−H348N (2.5 mg/mL) was crystallized without CoA in hanging drops at 22 °C using 167 mM sodium citrate (pH 6.5), 1.58 M $(NH_4)_2SO_4$, 1 mM EDTA, 1 mM NaN_3, and 1 mM DTT as well solution. Small crystals were obtained in two days.

Data Collection, Data Processing, and Structure Refinement. The data sets of the variants N316A, N316D, H348A, and H348N complexed with CoA were obtained by soaking the crystals in a cryosolution containing 20−25% glycerol and 4 mM CoA in the respective mother liquors for 1 min before cooling in liquid nitrogen. The variants N316H−H348N and N316H were cooled in liquid nitrogen after equilibration for 1 min in a cryosolution containing 25% glycerol in mother liquor. All data sets were collected at the ESRF (Table 1). All the data

sets, except the double mutant N316H−H348N data set, were processed with XDS (*31*). For the double mutant, data processing was performed with iMOSFLM (*32*) and SCALA (*33*). The space group of the crystals of each of the six crystallized variants is P21, like the wild type protein, with also similar cell dimensions (Table 1). The data processing statistics are shown in Table 1. The molecular replacement calculations were performed with PHASER (*34*) or MOLREP (*35*) from the CCP4 package (*36*), using the protein part of the 1DLU structure (*12*) as a model, with active site residues mutated into alanines. Structures were refined iteratively with REFMAC5 (*37*) and model building in electron density maps with COOT (*38*). In the REFMAC5 refinement, NCS restraints were used, while the TLS option was not. For each of the five single point mutation variants, additional rounds of refinement and solvent building were carried out with phenix. refine (*39*) with TLS parametrization. The final refinement statistics are shown in Table 1.

Thiolase Assays. All assays were done with freshly purified samples. All the kinetic assays were measured with PowerWaveX microplate spectrophotometer. Samples were mixed just before the first measurement. A negative control without enzyme was included in the measurements and taken into account in the calculations of the reaction rates. The concentrations of substrates (CoA, acetyl-CoA, and acetoacetyl-CoA) were determined by Ellman's test (*40*). For acyl-CoAs, a reaction mixture without hydroxylamine was used as a blank. When measuring the concentrations of CoA also a blank was used, being pure water instead of the CoA solution.

Thiolase activity for the thiolytic direction was measured by following the degradation of substrate, acetoacetyl-CoA, using the Mg^{2+} method (*29*, *30*) at 25 °C with few modifications. The reaction buffer consisted of 50 mM Tris-HCl (pH 8.1), 20 mM $MgCl_2$, and 60 μM CoA. The amount of acetoacetyl-CoA was varied for measurements of K_m and V_{max} in the range of 5−70 μM, and the total reaction volume was 0.3 mL. The change in absorbance at 303 nm was followed for 7 min after addition of an appropriate amount of enzyme (ranging from 5 ng of the wild type to several micrograms of protein for the inactive mutated variants). At 303 nm, the disappearance of the Mg^{2+}−acetoacetyl-CoA complex was measured. The absorption coefficient of this complex is 16900 M^{-1} cm^{-1}

Thiolase assays in the synthetic direction were performed at 30 °C, as described earlier (*30*, *41*). Briefly, the reaction was started by addition of the enzyme to the reaction mixture, in a total volume of 0.3 mL, containing 50 mM Tris-HCl (pH 7.4), 0.2 mM NADH, 1 unit of L-3-hydroxyacyl-CoA dehydrogenase, 0.5 mM DTT, and acetyl-CoA in the range of 0.1−1.5 mM. The rate of disappearance of NADH was followed at 340 nm, using as an extinction coefficient 6220 M^{-1} cm^{-1}. For the rather unreactive variants, the activity was measured at relatively low substrate concentrations (0.1−0.3 mM acetyl-CoA) to be able to obtain the k_{cat}/K_m value from the slope of the Michaelis−Menten curve (*21*). The amount of enzyme added ranged from 50 ng for wild type to several micrograms for the inactive variants.

Mass Spectrometric Studies. To verify, qualitatively, unexpected catalytic properties, for example thioesterase activity, of the new variants, a mass spectrometric analysis was done for wild type and three variants. A sample of the assay mixture (50 mM Tris-HCl; pH 8.1, 20 mM $MgCl_2$) in the presence of 60 μM acetyl-CoA was combined with 2,5-dihydroxybenzoic acid (50:50) and analyzed by the laser ionization method with a MALDI-TOF (Voyager-DETM STR biospectometry workstation, Applied Biosystems) instrument. The samples were taken from the assay mixture after 5 min of equilibration of 50 ng enzyme per 0.3 mL assay mixture. As a negative control, measurements were done without enzyme, and as a positive control, measurements were done in the presence of 60 μM CoA and 60 μM acetoacetyl-CoA.

Isothermal Titration Calorimetry. The CoA binding constants of the active site variants were determined at 25 °C with isothermal titration calorimetry (ITC), as previously described for the wild type enzyme (*42*). All the measurements were done in buffer containing 100 mM Tris-HCl (pH 7.4), 5% glycerol, and 1 mM DTT. In the standard measurement, the protein concentration was 50 μM and the CoA, used as a titrant, was at 5 mM concentration. The only exception was the C89A variant, for which 100 μM protein concentration was used. Titrations were performed with the VP-ITC microcalorimeter (MicroCal Incorporated), and the data were analyzed using the MicroCal Origin software. The binding ratio was fixed at one CoA molecule per active site.

Circular Dichroism Spectroscopy. Circular dichroism (CD) spectroscopy was performed at pH 7.4. The CD spectra were measured between 260 and 190 nm, using the Jasco J-715 spectropolarimeter. The buffer used was 10 mM potassium phosphate buffer, pH 7.4, and protein concentration was 0.1 mg/mL. The melting temperatures of the proteins were determined by heating the protein solution at 1 °C/min and recording the absorbance of polarized light at 222 nm. The melting point was determined to be the temperature at which 50% of the protein is unfolded.

Structure Analysis. The crystal structures of the new variants were compared with the structures of several wild type and mutant *Z. ramigera* thiolase complexes. For all these structures, the space group and crystal packing are the same, and there is one homotetramer per asymmetric unit. Because of the crystal packing of this crystal form, subunits A and B are better defined than subunits C and D (*12*). For the comparisons, subunit B has been used. The most important structure for these comparisons is that of the acetylated enzyme complexed with acetyl-CoA (1DM3, 2.0 Å resolution (*12*)), also referred to as the 1DM3 structure. The following structures were also used for the comparisons: 1DLU (2.25 Å resolution, the apo structure (*12*), and 1DLV (2.29 Å resolution, complexed with CoA (*12*)). Furthermore, the PDB entries 1M3Z (1.87 Å resolution, acetyl-CoA complexed with the C89A variant (*7*)), 1M1O (1.95 Å resolution, acetoacetyl-CoA complexed with the C89A variant (*7*)), 1M4S (1.87 Å resolution, acetylated enzyme (*7*)), and 2VTZ (2.3 Å resolution, complex of CoA and the C89A variant (*42*)) were used. All superpositions were done with the SSM method of Krissinel (*43*), as implemented in COOT (*38*).

RESULTS AND DISCUSSION

Kinetic Studies Concerning the Claisen Condensation Reaction of the Synthetic Direction. In the synthetic direction, the Claisen condensation reaction is known to be the rate limiting step (*41*, *44*). The intermediate, from which this reaction is initiated, has been trapped at low pH in a crystal structure as a complex of acetyl-CoA with acetylated thiolase (PDB entry 1DM3 (*12*)). In the corresponding competent complex (at basic pH) (Complex V, Figure 1B), Cys378 is negatively charged and His348 is assumed to carry a positive charge (Figure 1). The Claisen condensation reaction is initiated by the abstraction of the α-proton of acetyl-CoA by the deprotonated Cys378. SG(Cys378) is via two waters, Wat82 and Wat49, hydrogen

Table 1: Data Collection and Refinement Statistics

	N316A	N316H	N316D	H348A	H348N	N316H−H348N
data collection statistics						
space group	*P*21	*P*21	*P*21	*P*21	*P*21	*P*21
unit cell parameters						
a (Å)	84.6	84.5	84.7	84.3	84.7	84.2
b (Å)	79.2	79.5	79.3	79.1	79.2	79.9
c (Å)	148.7	147.7	151.0	149.4	153.0	149.9
β (deg)	92.8	91.5	95.6	92.7	92.5	92.9
temp (K)	100	100	100	100	100	100
wavelength (Å)	0.9334	0.9334	0.9334	0.9334	0.9334	0.9334
resolution (Å)[a]	20.0−2.0 (2.20−2.0)	20.0−2.3 (2.5−2.3)	20.0−2.5 (2.65−2.5)	20.0−1.8 (1.95−1.8)	20.0−1.8 (1.95−1.8)	43.9−3.0 (3.14−3.0)
R_{merge} (%)	15.7 (48.8)	10.5 (30.0)	15.4 (51.0)	10.5 (47.1)	11.8 (46.1)	13.9 (33.8)[b]
completeness (%)	99.2 (98.1)	99.6 (99.6)	99.7 (99.8)	99.6 (99.5)	98.6 (97.2)	97.4 (95.1)
I/σ(I)	9.7 (4.1)	11.1 (4.7)	9.2 (3.1)	10.5 (3.2)	9.1 (3.0)	6.8 (2.3)
no. of unique reflections	132297	86887	69019	181049	184515	39685
redundancy	4.0 (3.9)	3.7 (3.7)	4.2 (4.1)	4.0 (3.8)	3.9 (3.7)	7.4 (7.3)
mosaicity (deg)	0.24	0.29	0.24	0.26	0.24	1.1
B factor from Wilson plot (Å^2)	20.1	25.1	24.6	21.1	19.8	26.6
ESRF beamline	ID14-1	ID14-2	ID14-1	ID14-1	ID14-1	ID14-1
PDB entry[e]	2WKT	2WKU	2WKV	2WL4	2WL5	2WL6
refinement statistics						
resolution (Å)	19.6−2.0	20.0−2.3	19.7−2.5	19.6−1.8	19.4−1.8	37.4−3.0
no. of reflections	132285	86886	69015	180999	184508	39191
R_{factor} (%) for the working set	18.7	20.1	17.3	23.1	22.1	23.2
R_{free} (%) for the test set	23.6	25.8	23.8	27.0	25.7	29.1
no. of protein atoms (A, B, C, D)	11299	11266	11260	11331	11332	11252
no. of water atoms	1345	630	786	1170	1234	26
no. of CoA atoms in A and B subunits	96		96	96	96	
no. of other solvent atoms	45 SO_4	45 SO_4	50 SO_4	125 SO_4	70 SO_4	
	1 K^+	48 glycerol	2 Na^+	3 Na^+	1 Na^+	
	1 Na^+			3 Cl^-	1 Cl^-	
	1 Cl^-				48 glycerol	
rmsd for bond distances (Å)	0.009	0.005	0.006	0.008	0.009	0.012
rmsd for bond angles (deg)	1.2	0.9	1.0	1.1	1.1	1.5
rmsd for *B* factors						
B factors main chain (Å^2)	2.5 (A)	3.7 (A)	3.4 (A)	2.2 (A)	2.2 (A)	0.4 (A)
	2.5 (B)	3.7 (B)	3.3 (B)	2.2 (B)	2.2 (B)	0.4 (B)
	2.6 (C)	3.7 (C)	3.4 (C)	3.2 (C)	3.1 (C)	0.3 (C)
	2.9 (D)	3.8 (D)	3.4 (D)	4.1 (D)	3.1 (D)	0.3 (D)
B factors side chain (Å^2)	3.8 (A)	5.1 (A)	5.1 (A)	3.7 (A)	3.7 (A)	0.6 (A)
	3.9 (B)	4.9 (B)	4.7 (B)	3.9 (B)	3.6 (B)	0.7 (B)
	3.8 (C)	4.9 (C)	4.8 (C)	3.9 (C)	3.4 (C)	0.6 (C)
	3.5 (D)	4.3 (D)	4.7 (D)	4.8 (D)	3.2 (D)	0.6 (D)
average *B* factors						
protein (side chain + main chain) atoms (Å^2)	13.3 (A)	25.9 (A)	14.6 (A)	16.5 (A)	16.2 (A)	22.8 (A)
	13.1 (B)	25.5 (B)	14.8 (B)	16.3 (B)	15.8 (B)	21.1 (B)
	29.1 (C)	48.1 (C)	30.7 (C)	68.4 (C)	53.5 (C)	24.4 (C)
	35.7 (D)	52.7 (D)	34.9 (D)	67.1 (D)	61.7 (D)	25.0 (D)
water molecules (Å^2)	32.1	39.1	26.3	35.9	35.6	6.5
CoA atoms (Å^2) in A and B subunits	30.6		36.6	40.3	34.9	
NCS rmsd for Cα atoms (Å)	0.2 (A/B)	0.3 (A/B)	0.2 (A/B)	0.4 (A/B)	0.3 (A/B)	0.5 (A/B)
	0.3 (A/C)	0.4 (A/C)	0.3 (A/C)	0.7 (A/C)	0.4 (A/C)	0.6 (A/C)
	0.3 (A/D)	0.4 (A/D)	0.3 (A/D)	0.5 (A/D)	0.4 (A/D)	0.6 (A/D)
Ramachandran plot[c]						
favored (%)	97.3	96.4	96.2	94.2	96.4	91.6
allowed (%)	2.7	3.3	3.5	5.0	3.5	7.9
others		0.3	0.3	0.8	0.1	0.5
comments: outliers (in subunit A and B)		Met 134 (A)[d]	Thr 240 (A)[d]	Gly 131 (B)[d]		Pro349 (A)[d]

[a]The numbers in parentheses refer to the highest resolution shell. [b]R_{pim} (all I+ and I−) is reported, as calculated by SCALA (*33*). [c]Calculated by using the program Molprobity (*57*). [d]These outliers are always very close to the allowed region. [e]The following PDB entries refer to the described crystal structures: 2WKT (N316A), 2WKU (N316H), 2WKV (N316D), 2WL4 (H348A), 2WL5 (H348N) and 2WL6 (N316H-H348N).

bonded to ND2(Asn316) and O(Asn316), respectively. SG-(Cys378) is also within hydrogen bonding distance of O(Cys378), but the precise geometry is very poor for hydrogen bonding. Figure 4A visualizes the expected hydrogen bonding scheme in the competent active site complex, in which Cys378 is deprotonated. In the Claisen condensation proton abstraction step, an

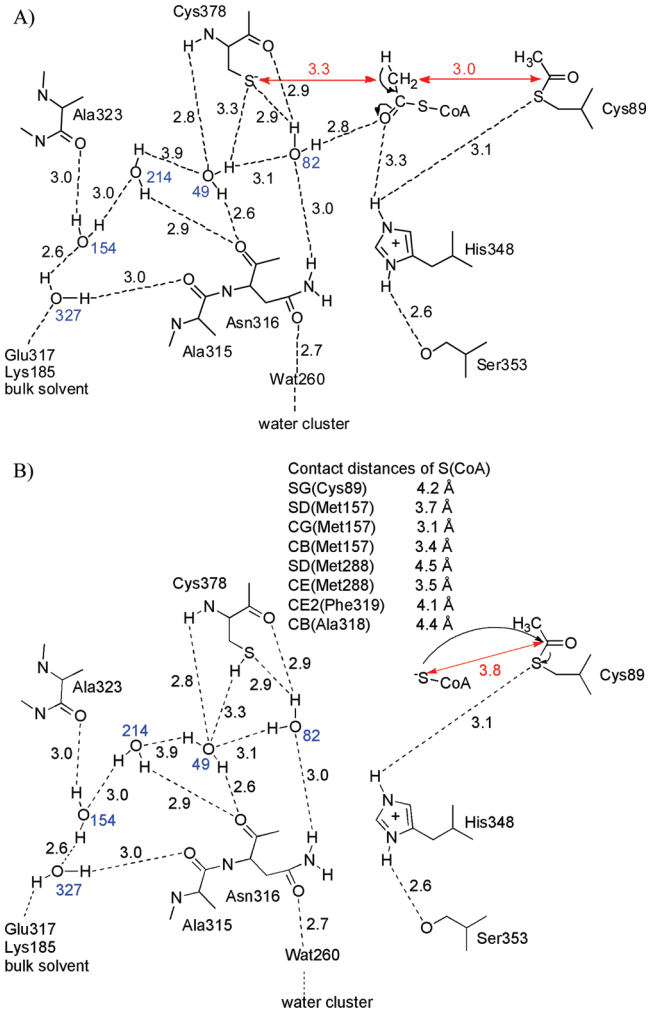

FIGURE 4: Two possible hydrogen bonding schemes in the thiolase active site. All distances are in Å. The red arrows highlight critical active site distances. The striped lines indicate the hydrogen bonds; the indicated distances always refer to the distances between hydrogen bond donor and acceptor. (A) The competent active site of complex V for the Claisen condensation reaction (clockwise step 5, Figure 1B). The deprotonated Cys378 abstracts a proton from the methyl-group of acetyl-CoA to initiate the reaction. The oxyanion hole I for stabilizing the enolate intermediate is formed by the Asn316-Wat82 dyad and NE2(His348). The electrophilicity of Wat82 is enhanced by the donor hydrogen bond of Asn316. The geometric information is taken from PDB entry 1DM3. The black arrows indicate the movement of the electrons when the α-methyl group is deprotonated and the enolate is formed. (B) The competent active site for the acetyl transfer reaction between Ac-Cys89 and the CoA-S atom, when thiolase is operating in the thiolytic direction (step 2 of Figure 1B, counterclockwise direction). The visualized intermediate is complex III (Figure 1B) once the incoming CoA has been deprotonated. In the thiolase complexes, the CoA-S atom is tightly anchored and well positioned for nucleophilic attack on the carbonyl carbon atom of the acetylated cysteine. The contact distances (within 4.5 Å) between the CoA-S atom and the protein are provided. The geometric information is taken from PDB entry 1DM3. The black arrows indicate the movement of the electrons when the acetyl group is transferred to CoA.

enolate is formed, with a negative charge on the enolate oxygen (Figure 2). This oxyanion will be stabilized by hydrogen bonding interactions with Wat82 of the Wat82-Asn316 diad and NE2-(His348), which form oxyanion hole I.

The interactions in oxyanion hole I were tested by mutating Asn316 and His348. Subsequently, the enzymological and structural properties of these variants were determined. The kinetic

Table 2: Kinetic Data for the Condensation Reaction Using Acetyl-CoA as the Substrate[a]

	catalytic triad	K_m (acetyl-CoA) (μM)	k_{cat} (sec^{-1})	k_{cat}/K_m[b] (mM^{-1} s^{-1})	$\Delta\Delta G^{\ddagger}$[c] kcal/mol
wild type	CNH	455 ± 35	38 ± 5	60	
N316D	CDH			inactive	
N316A	CAH			0.1	3.8
N316H	CHH			0.2	3.4
H348A	CNA			0.05	4.3
H348N	CNN			0.2	3.4
N316H−H348N	CHN	263 ± 29	0.9 ± 0.1	2.0	2.0

[a]The kinetic constants were derived from two or more independent experiments. Only for wild type and the double mutant, enough data points could be collected to determine directly the values of k_{cat} and K_m from the Michaelis−Menten curve. [b]The tabulated k_{cat}/K_m values have been obtained from the slope of the Michaelis−Menten curves at low substrate concentration, normalized for the enzyme concentration. [c]The $\Delta\Delta G^{\ddagger}$ values have been calculated from the k_{cat}/K_m ratios of mutant and wild type (21), as explained in the text.

data of the condensation reaction (Table 2) show that the k_{cat}/K_m values are 600-fold and 300-fold lower for the N316A and N316H variants, respectively, whereas for the N316D variant, catalytic activity is not detectable. For N316A, N316H, and N316D, it was verified by mass spectrometry that unexpected degradative catalytic activities on acetyl-CoA were not introduced by these mutations. These mass spectrometric measurements were done as described in the Experimental Procedures section by incubating these variants in the assay mixture in the presence of acetyl-CoA. Degradation of acetyl-CoA by these three variants could not be shown.

The H348A and H348N variants also have 1200- and 300-fold lower k_{cat}/K_m values than the wild-type enzyme, respectively. For these Asn316 and His348 single point mutation variants, the $\Delta\Delta G^{\ddagger}$ values range from 3.4 to 4.3 kcal/mol. The simplest explanation for this increase of the transition state barrier is to propose that only the oxyanion hole stabilization is disabled in these variants, whereas all other interactions important for catalytic function remain intact, implying that the $\Delta\Delta G$ values (Table 2) refer to the changed reactivity of the acetylated enzyme in the condensation step. This requires that only minimal structural rearrangements are induced by the mutations. To test this hypothesis, crystal structures were determined for each of the variants, as outlined below.

Structural Properties of the New Variants. Each of the thiolase variants has similar stability to the wild type thiolase, as measured by CD melting experiments, with the T_m values ranging from 58 to 65 °C, with the wildtype having a T_m of 62 °C. The crystal structures of the variants were determined at resolutions ranging from 1.8 to 3 Å (Table 1). Table 3 summarizes some of the key structural data. Only minor structural changes affecting the side chain conformations and the active site water molecules were found, as described in more detail in the subsequent paragraphs. For all comparisons, subunit B is used. Unless otherwise mentioned, the structures are compared with the 1DM3 structure.

N316A (Liganded with CoA). In this structure, CoA is well-defined by the electron density. The CoA-sulfur atom is bound slightly deeper (0.5 Å) as in wild type thiolase, and the two active site waters, Wat49 and Wat82, are present at high occupancy, at

the same place as in the wild type active site (Figure 5 and Figure 6). Wat82 is missing the hydrogen bonding interactions with the wild type Asn316 side chain because of the N316A mutation. There is no change of the main chain of Ala316 and His348. An extra water replaces the OD1(Asn316) atom (like in N316H), and the side chain of His348 has rotated by 50° toward this water; its ND1-atom is hydrogen bonded to this new water. The His348 side chain is not hydrogen bonded anymore to the Ser353 side chain. Cys89 is oxidized to a sulfenic acid, and the extra sulfenic acid oxygen atom is bound in oxyanion hole II.

N316H (*Unliganded*). In this unliganded structure (Figure 6), the bulkier histidine side chain causes Wat49 to be moved to a slightly different position, still being hydrogen bonded to N(Cys378) and O(His316). Wat82 is absent in this structure, as the NE2(His316) atom occupies this site. An extra water replaces the OD1(Asn316) atom, like in the N316A structure. The side chain of His348 has slightly shifted (by 0.5 Å), but the hydrogen bond with Ser353 is still intact. Cys89 appears not to be oxidized, and the sulfur atom has rotated toward oxyanion hole II and is in the same position as in the unliganded, wild type structure (1DLU).

N316D (*Liganded with CoA*). In the structure of this variant, it is seen that the His348 side chain is rotated toward the Asp316 side chain (Figure 6), by approximately 90°, and NE2(His348) becomes hydrogen bonded to OD2(Asp316). The hydrogen bond of ND1(His348)-OG(Ser353) is lost. Wat82 appears to be absent but Wat49 is present. The main chain and side chain of Asp316 are slightly shifted, by 0.4 Å, away from His348. Cys89 and Cys378 have been modeled as being not oxidized, although the electron density map suggest that Cys89 might be partially oxidized. CoA is well-defined by its density and the sulfur atom is bound 1 Å deeper in the active site, as compared to the thiolase−CoA complex (1DLV) (*12*).

H348A (*Liganded with CoA*). There are no changes in the main chain structure near Asn316 and Ala348 (Figure 6). The side chain of Asn316 is positioned slightly closer to the Cys378 side chain. Both Wat82 and Wat49 are present, but for Wat49 there is only weak density. The reactive mercaptoethanolamine end of CoA is somewhat disordered, judged from the electron density map, and bound 1.6 Å deeper into the active site cavity, as has also been noted in a complex of CoA with the C89A variant (*42*). There is a water molecule in oxyanion hole II plus an extra water nearby. Cys89 appears to be in multiple conformations and/or partially oxidized, with the sulfenic oxygen atom pointing toward Ala348. Cys378 is also oxidized. Some extra waters fill up the space vacated by the H348A-mutation.

Table 3: Summary of the Available Structural Data

	catalytic triad	PDB code	ligand	resolution (Å)	predicted overall charge in the active site cavity
wild type	CNH	1DM3	acetyl-CoA/ acetylated-Cys89	2.0	0
wild type	CNH	1DLV	CoA	2.3	0
wild type	CNH	1DLU		2.3	0
N316D	CDH	2WKV	CoA	2.5	−1
N316A	CAH	2WKT	CoA	2.0	0
N316H	CHH	2WKU		2.3	0
H348A	CNA	2WL4	CoA	1.8	−1
H348N	CNN	2WL5	CoA	1.8	−1
N316H−-H348N	CHN	2WL6		3.0	0

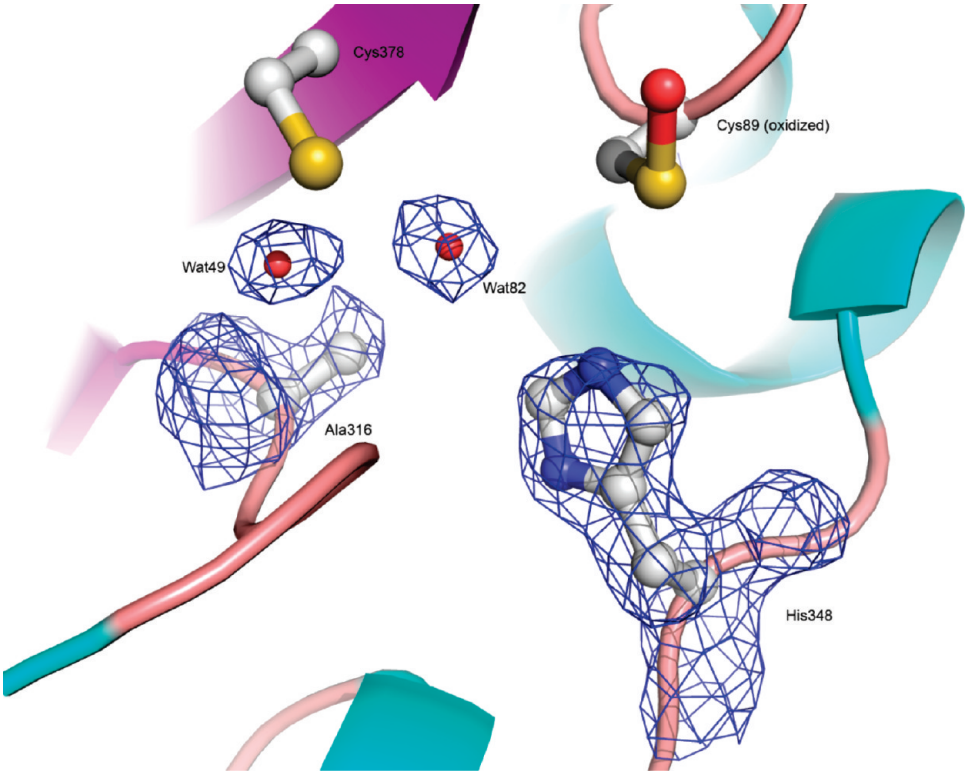

FIGURE 5: N316A structure, complexed with CoA. The map is an $(F_o - F_c)\alpha_c$ omit map, calculated after omit refinement, leaving out residues 316 and 348 as well as the two waters. The map is contoured at 2.5σ.

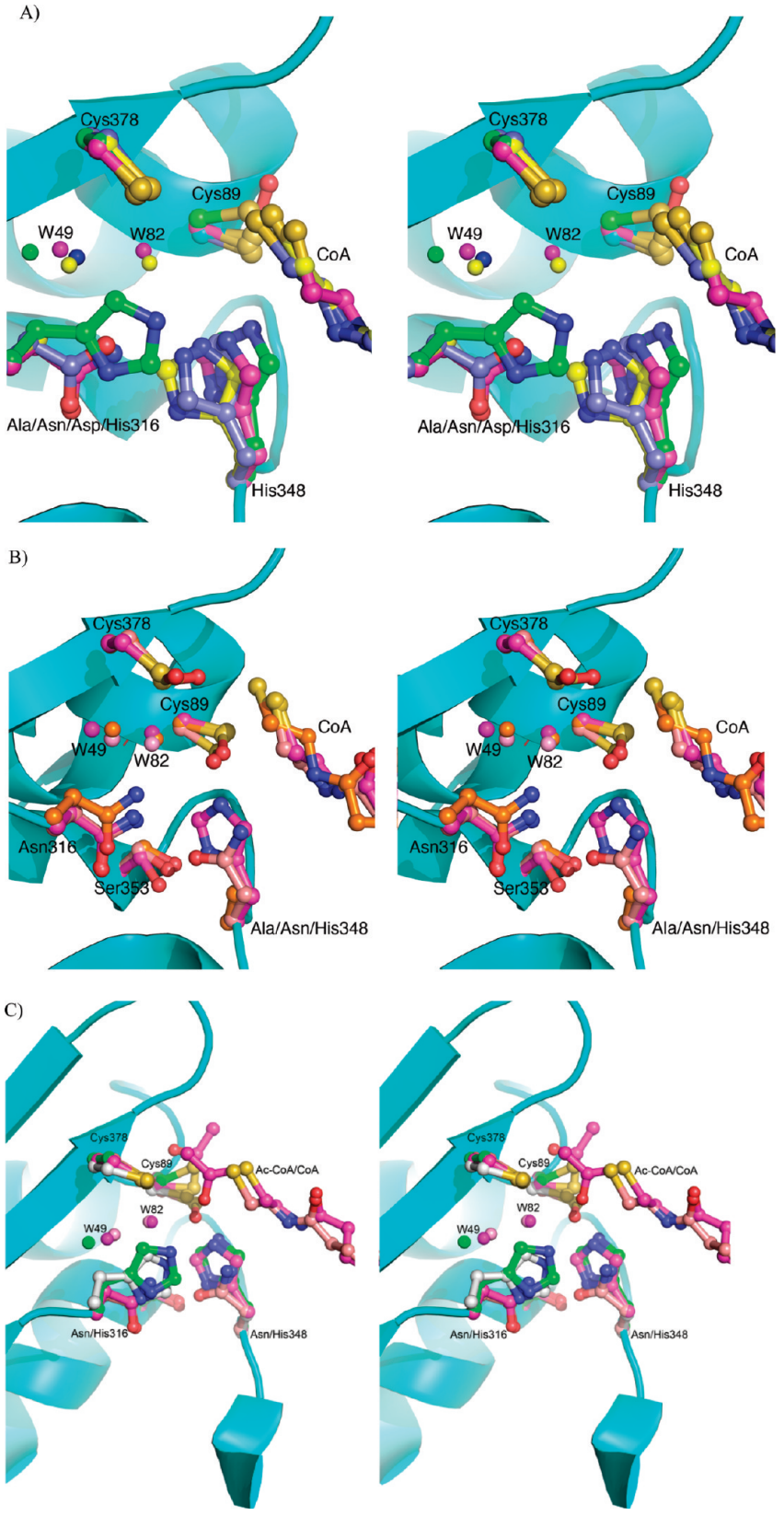

FIGURE 6: Comparison of the active site geometries of the variants. (A) Stereo view of the active sites of the N316A (yellow), N316H (green), and N316D (blue) variants, together with the structure of the wild type thiolase complexed with CoA (1DLV, magenta)). (B) Stereo view of the active sites of the H348A (orange) and H348N (pink) variants, together with the structure of the wild type thiolase complexed with CoA (magenta, 1DLV). (C) Structures of the four possible combinations of the catalytic triad, i.e., CNH (magenta, wild type, PDB entry 1DM3), CHH (green, the N316H variant, unliganded), CNN (pink, the H348N variant, liganded), and CHN (gray, the double mutation variant, unliganded).

H348N (*Liganded with CoA*). There are no changes in the main chain structures near residues 316 and 348 (Figure 6). Also the side chain conformation of Asn316 is unchanged. The CoA molecule is well-defined by the electron density map, and the mode of binding is similar to the wild type. Wat82 and Wat49 are well-defined in the maps, being located in the same place as in

wild type. From the hydrogen bonding scheme, it appears that the OD1(Asn348) is hydrogen bonded to ND2(Asn316). OD1-(Asn348) is also hydrogen bonded to Ser353. The Cys89 side chain is oxidized, and its sulfenic oxygen atom points toward Asn348. Cys378 seems also partially oxidized. Like in the H348A structure, there is a water molecule in oxyanion hole II plus an extra water nearby.

N316H−H348N (*Unliganded*). Only small changes in the main chain are observed, together with small changes in the side chain orientations (Figure 6). The data of this crystal structure extends only up to 3 Å resolution, and therefore, the water structure is not well-defined. The catalytic cysteines appear not to be oxidized. Like in the N316H structure, it is seen that NE2-(His316) is at hydrogen bonding distance from SG(Cys89) and, therefore, could act as the base activating Cys89.

The side chains of Asn316 and His348 closely interact with each other (Figure 3). Indeed, in each of the structures of these point mutation variants, the conformation of the nonmutated neighboring residue has changed somewhat, except for the H348N variant, where the Asn316 conformation has not changed. Also Wat82 and Wat49 are located in the same place in this variant as in N316A, H348A, and H348N. Wat49 is present in each of the structures, whereas in N316D, Wat82 has not been included in the model. In the structures cocrystallized with CoA, Cys89 is partially or completely oxidized (to a sulfenic acid). Also, Cys387 is sometimes partially oxidized. These oxidations could be induced by radiation damage, but oxidation of Cys89 has also been observed in case of cocrystallization experiments with the native thiolase (*42*) and is correlated with the relatively long time between setting up the crystallization and harvesting the crystals. It is only seen with cocrystallizations in the presence of CoA: apparently the presence of CoA increases the oxidation sensitivity of the active site cysteines, both in wild type as well as in the variants. In wild type thiolase, this oxidation seems to be a slow process. This observation has also been made in the studies of the T2-thiolase (*30*). As all kinetic data is determined from freshly prepared enzyme, this phenomenon is unlikely to interfere with the kinetic measurements. In fact the significant variation in K_m of acetoacetyl-CoA as measured in the degradative kinetics also suggest that the mutations modulate the acetoacetyl-CoA affinity, which is not caused by possible cysteine oxidations, as this would irreversibly inactivate the enzyme and only effect the k_{cat}.

In all structures, the mode of CoA binding is found to be the same as in wild type, but such that the CoA-sulfur atom in most cases is bound slightly deeper into the active site cavity, except for the H348A crystal structure in which case the CoA sulfur atom binds more than 1.5 Å deeper into the active site.

The small structural changes induced by the point mutations (Figure 6) have remarkably decreased the catalytic efficiency of the new variants (Table 2) when assaying for the condensation direction. Except for the H348N mutant, the geometry of both hydrogen bond donors of oxyanion hole I is affected by the point mutations. The energetic contribution from hydrogen bonding interactions critically depends on the precise geometry (*45*). Indeed, our kinetic data clearly show the importance of these small changes of oxyanion hole I for the transition state stabilization. The catalytic proficiency will also depend on the charge distribution in the active site. In some variants (N316D, H348A, and H348N), this charge distribution is different (Table 3). The N316D variant is completely inactive, probably also because in the active site hydrogen bonding scheme, Asp316 will be a hydrogen bonding acceptor instead of a donor, as in wild type. In addition, the electrostatic environment with a negative charge on the Asp316 side chain will disfavor the formation of the negatively charged enolate intermediate of the Claisen condensation reaction. For the double mutant, His316 is hydrogen bonded to Cys89, and therefore, it can act as the base activating Cys89 and become positively charged, resulting in the same net charge in the active site as for wild type (Table 3).

Table 4: Kinetic Data for the Thiolytic Reaction Using Acetoacetyl-CoA as the Substrate[a]

	catalytic triad	K_m (acetoacetyl-CoA) (μM)	k_{cat} (s^{-1})
wild type	CNH	24 ± 5	813 ± 125
N316D	CDH		
N316A	CAH	14 ± 4.7	43 ± 7.5
N316H	CHH	12 ± 3.2	181 ± 17
H348A	CNA	9 ± 1.8	0.6 ± 0.08
H348N	CNN	15 ± 2.7	6 ± 2.7
H348N−N316H	CHN	14 ± 1.5	20 ± 1

[a]The kinetic constants were derived from two or more independent experiments, using a constant CoA concentration of 60 μM.

Kinetic Analysis of the Thiolytic Reaction. The effects of the mutations on the thiolytic reaction were also analyzed. The enzyme is more proficient in the thiolytic direction, and therefore, it turned out to be possible to measure both affinity (expressed as K_m) as well as catalytic rates (k_{cat}) (Table 4) for each of the variants, except for N316D. In this assay, the observed K_m is in fact an apparent K_m, as it will also depend on the used concentration of CoA in the assay. In the thiolytic direction, the chemistry and the rate limiting step are very different from the synthetic direction: the transfer of the acetyl group from Cys89 to CoA is the rate limiting step (*41*, *44*). This is the reverse reaction of step 2 of Figure 1B. In this counterclockwise direction, the deprotonated CoA sulfur moiety nucleophilically attacks the carbonyl carbon atom of the acetylated enzyme (step 2 (counterclockwise), Figure 1B). The deprotonated CoA−SH moiety is generated via proton abstraction, for example by Cys378; in the active site the S(CoA)−S(Cys378) distance is 5.3 Å, and the S(CoA)−Wat82 distance is 5.2 Å. The deprotonation will be favored by the positively charged His348 side chain, where (S(CoA)−NE2(His348) is 4.7 Å. The precise geometry and electrostatics of the active site will affect the reactivity of the CoA sulfur anion in the complex of the acetylated enzyme. The proposed hydrogen bonding scheme for the active site, competent for acetyl-transfer to CoA, is shown in Figure 4B.

For each of the variants, the affinity for the substrate acetoacetyl-CoA, as measured by the K_m, is higher than in wild type (Table 4). In the N316D variant, the electrostatics and the hydrogen bonding scheme of the active site will be different due to the negative charge of Asp316, causing the catalytic efficiency to remain below the assay detection limit. The variants with the lowest catalytic rates are those in which the charge and electrostatics of the active site are different from wild type: N316D, H348N, and H348A. The latter mutation has also been studied in rat T1 thiolase (*46*), where a 1000-fold decreased turnover number of the thiolytic kinetics was observed.

CoA Binding by the New Variants. The affinity of the new variants toward CoA was also measured by ITC (Table 5). Each

Table 5: Calorimetric Analysis of CoA Binding[a]

	K_d (CoA) (μM)	K_d (acetyl-CoA) (μM)
wild type	81 ± 29[b]	
C89A	307 ± 64[b]	496 ± 33
N316D	128 ± 9	
N316A	49 ± 3	
N316H	85 ± 5	
H348A	64 ± 4	
H348N	30 ± 2	
H348N−N316H	32 ± 3	

[a]Each experimental result is an average of at least two measurements. [b]As measured previously by Meriläinen et al. 2008 (*42*).

of the variants has high affinity for CoA, despite the much reduced catalytic efficiencies, indicating that the CoA binding properties of the new variants remain relatively intact. The binding constants for acetyl-CoA and CoA were also measured for the inactive C89A variant (Table 5), showing that the affinities of this variant for CoA and acetyl-CoA are very similar. This observation indicates that the interactions of the thioester oxygen atom do not significantly contribute to the affinity of acetyl-CoA. This conclusion is also consistent with the kinetic data of the catalysis in the degradative direction (Table 4), indicating similar affinity for acetoacetyl-CoA in the variants and wild type thiolase. Apparently, disabling oxyanion hole I affects the Claisen condensation reaction efficiency (Table 2) but not the substrate affinity. Thus, the oxyanion hole I interactions are important for interactions with the Claisen condensation transition state but not for interactions with the substrate.

The Altered Hydrogen Bonding Properties of the Mutated Oxyanion Hole I. The active site of thiolase is deeply buried at the end of the pantetheine binding tunnel. The catalytic cavity is very polar, and the charge distribution and hydrogen bonding schemes change during the catalytic cycle. The side chains of Asn316 and His348 play a key role in this geometry. Therefore, it is important to assign protonation states and hydrogen bonding interactions of the active site for each of the discussed intermediates. For the wild type competent active site, when focusing on the Claisen condensation reaction, the likely hydrogen bonding scheme and charge distribution are visualized in Figure 4A. In the N316D mutant, it can be assumed that the aspartate is in the unprotonated, negatively charged state at the pH of the assay conditions. Therefore, in this variant, the electrostatics as well as the hydrogen bonding scheme will be different from wild type. In the H348A and H348N variants, the overall charge in the active site is also different from the wild type enzyme, the positively charged histidine side chain being replaced by a neutral side chain. Therefore, for the comparison of the relative catalytic efficiencies of the mutants with respect to wild type, it is most informative to consider the N316A and N316H variants. For these two variants, the catalytic efficiency of thiolysis is 11-fold and 2-fold decreased, whereas in the condensation direction, the decrease is 600-and 300-fold, respectively. Apparently, the structural changes in oxyanion hole I in these two variants are sufficiently small, such that the thiolytic kinetics is not much affected, whereas the changes are sufficiently large for the oxyanion hole I stabilization in the condensation reaction to be critically disabled (Table 2). In the synthetic direction, the interpretation of the data is facilitated by the assumption that the rate limiting step will be the same for each of the variants, i.e., the Claisen condensation step (step 5 in Figure 1B). Focusing on N316A and N316H, it should be noted that in the N316H variant, Wat82 is missing, as its position corresponds to NE2(His316). In N316A, Wat82 is present (Figures 5, 6) but the His348 side chain is rotated away by 50° from its wild type position. In the wild type complex, Wat82 provides a hydrogen bond donor interaction to the thioester oxygen atom of the transition state and to O(Cys378) (Figure 4A). Wat82 accepts a hydrogen bond from ND2(Asn316) and Wat49. In the N316A complex, the electrophilicity of Wat82 will be reduced due to the loss of the interaction with ND2(Asn316). The kinetics of N316A in the condensation reaction show that oxyanion hole I is disabled, but the crystal structure indicates that this disabling comes from small changes affecting both hydrogen bond donors of this oxyanion hole, i.e., Wat82 and NE2(His348). This disabling destabilizes the transition state by 3.8 kcal/mol (Table 2), whereas the affinity of the substrate is not affected. Although this number compares well with the kinetic data of Fersht et al. (*20*), for the loss of one charged hydrogen bonding interaction, the combined structural and kinetic data suggest that the destabilization effect seen is most likely a concerted effect of both hydrogen bond donors of oxyanion hole I.

The kinetic properties in the condensation direction are the least affected in the double mutant. The affinity of the substrate, acetyl-CoA, is slightly higher (Table 2) than for wild type, as also noted for the substrate, acetoacetyl-CoA, of the thiolytic degradative step (Table 4). Apparently, in this variant, the key features of the competent oxyanion hole I are best preserved. NE2(His316) is in hydrogen bonding distance of SG(Cys89) and can, therefore, facilitate the deprotonation and activation of Cys89. Consequently, His316 is assumed to be doubly protonated and positively charged during the catalytic cycle. Therefore, in this active site, the overall charge and electrostatics are predicted to be the same as in wild type. Furthermore, in this variant, NE2(His316) replaces Wat82 and ND2(Asn348) replaces NE2(His348), thereby mimicking better than any of the single point mutants a catalytically competent oxyanion hole I.

Implications for the Thiolase Reaction Mechanism. His348 is proposed to have a dual role in the reaction mechanism, being important for the activation of the catalytic cysteine (reaction 1, Figure 1) and for generating oxyanion hole I. The latter functionality is consistent with the condensation kinetics and the structural data. The kinetic data on the thiolytic direction shows the largest decrease in catalytic efficiency for the N316D and H348A variants. In the N316D variant, the electrostatics and hydrogen bonding interactions in the active site will be rather different from wild type, and therefore, this variant gives no specific information on the importance of His348. Interestingly, for the H348A variant, very low thiolytic activity was detected. Although the structural analysis indicates that in this complex, the reactive end of the CoA is bound differently, it seems likely that the deprotonation of Cys89 has become much less efficient in this variant. It can be noted (Table 4) that, in the N316A and N316H variants, the thiolytic efficiency is much less affected than in the H348A and H348N variants, whereas in the condensation direction, each of the variants have similarly reduced catalytic efficiencies. In each of these four variants, the hydrogen bonding geometry of oxyanion hole I is affected, whereas only for H348A and H348N, also the activation mechanism of Cys89 is affected. These data confirm that proper hydrogen bonding geometry in

oxyanion hole I is critically important for the Claisen condensation reaction, whereas for the thiolytic reaction, Cys89 deprotonation could become the rate limiting step in the H348A and H348N variants, in good agreement with a dual functionality of His348.

In the Claisen condensation reaction, as catalyzed by thiolase, the stereochemistry involves an inversion at the methyl group of acetyl-CoA (*47*). The abstraction of the methyl proton, the enolization step (reaction 5, Figure 1), is distinct from the condensation reaction (*48*). Abstracting a proton from the methyl group is difficult; the pK_a of the α-methyl group of a thioester is very high, around 21 (*49*), whereas the pK_a of the base, the cysteine side chain, is around 9. The specific active site geometry changes the pK_a values of the reactive groups and thereby allows for the proton transfer reaction. In thiolase, the pK_a and reactivity of Cys378 will, in turn, be modulated by Wat82 and Wat49. The proposed hydrogen bonding schemes of these two waters are visualized in Figure 4. Wat49 is anchored between N(Cys378) and O(Asn316) and is also hydrogen bonded to Wat82 and Wat214. Wat82 is also bridging between Cys378 and Asn316, being hydrogen bonded to O(Cys378) and ND2-(Asn316). Wat49 is further hydrogen bonded to a trail of water molecules, which extends toward the back of the molecule (Figure 3). Each of these waters, including Wat82 and Wat49, has at least one hydrogen bond interaction with a main chain oxygen atom. The hydrogen bonding schemes of these water molecules will be different for the active sites with anionic and neutral Cys378 side chains (Figure 4). In both schemes, the hydrogen bonds with the main chain atoms are preserved. During the Claisen condensation reaction, Cys378 is converted from the anionic form (complex V, Figure 1) to the neutral form (complex VI, Figure 1). In the most proficient thiolases, the *Z. ramigera* thiolase and the human cytosolic thiolase (CT) (*50*), Wat49 is hydrogen bonded to a trail of waters, in which case the switching of the hydrogen bonding scheme is facilitated by the presence of this adjacent water trail. In T2 thiolase, which has lower catalytic efficiency, only Wat82 and Wat49 are preserved (*30*).

Several kinetic studies have shown that the efficiency of deprotonation of the Cα proton of acetyl-CoA by thiolase is increased for the acetylated enzyme, compared to the nonacetylated enzyme (*44*, *48*, *51*). This observation agrees very well with the proposed hydrogen bonding schemes shown in Figure 4A (in the presence of bound acetyl-CoA) and Figure 4B (in the absence of bound acetyl-CoA). The binding of the thioester oxygen of acetyl-CoA to the acetylated enzyme in oxyanion hole I favors an active site hydrogen bonding scheme in which Cys378 is deprotonated. Therefore, the binding of this thioester oxygen atom in oxyanion hole I activates Cys378 for being the base for abstracting the Cα-proton of acetyl-CoA, as required in the Claisen condensation reaction.

Properties of the Oxyanion Holes of Other CoA-Dependent Enolizing Enzymes. In citrate synthase (*1*), another condensing enzyme, the Cα atom of acetyl-CoA forms a covalent C−C bond after reacting with the carbonyl carbon atom of the 2-keto group of oxaloacetate. This reaction is in fact an aldol condensation reaction, as the carbonyl oxygen atom is protonated after the formation of the C−C bond. In citrate synthase, like in thiolase, the enolization step of the Cα-atom of acetyl-CoA is the rate limiting step (*52*). The hydrogen bond donors of the corresponding oxyanion hole I are a water molecule (Wat585) and the NE2(His274) side chain atom. The active site of citrate synthase is more surface-exposed, and Wat585 is, via hydrogen bonding with a neighboring water molecule, hydrogen bonded to bulk water. Also for citrate synthase, it has been found that the thioester oxygen atom possibly does not contribute much to the affinity of the substrate. For example, the affinity of acetyl-CoA for wild type enzyme and the H274G variant is the same, although the reaction rates are much lower in the latter case (*23*). In the H274G variant, the transition state stabilization is 3.8 kcal/mol less than in wild type; no crystal structures of the mutated variant are available.

The importance of the oxyanion hole for enolization has also been studied for enzymes having the crotonase fold (*24*). In these enzymes, two main chain NH-groups provide the hydrogen bonding partners. For the rat hydratase enzyme, the importance of these hydrogen bonds for transition state stabilization and substrate binding has been probed by mutagenesis. The NH groups of Ala98 and Gly141 are the hydrogen bond donors, and the G141P variant, in which the hydrogen bonding capacity of one of the oxyanion hole partners has been disabled, is much less active, but the affinity remains the same (*53*). For this mutated variant of crotonase, no crystal structures are available of the unliganded or liganded states, but complementary experiments suggest that the fold and the mode of substrate binding are not affected. The studies on the properties of the G141P variant of crotonase (*53*) indicate that the contribution of this hydrogen bond to the transition state stabilization can be estimated as 8 kcal/mol.

The Importance of the CNH, CHH, and CHN Catalytic Triads. The presence of Wat82 and Wat49 is a conserved feature of the current set of structurally characterized active conformations of thiolases, which include the β-subunit of the bacterial fatty acid oxidation multienzyme-complex (*54*) and the yeast (*55*) peroxisomal A/B-thiolase. Wat82 is present in the structure of plant peroxisomal thiolase, which has been crystallized in an inactive conformation (*56*). Each of these thiolases belong to the CNH-class of thiolases. It is currently not known what water structure is present in the active site of the CHH category thiolases. In the other members of the superfamily of known structure, belonging to either the CHN or the CHH category, such as the KAS and PKS enzymes, Wat82 and Wat49 are not conserved, indicating that these two catalytic water molecules are unique for the CNH thiolases, including the *Z. ramigera* thiolase.

The CNN triad, represented by the H348N variant, has not been observed in a wild type enzyme of the thiolase superfamily. In this superfamily of enzymes, the enolate transition state is negatively charged (Figure 4). In the presence of a histidine in the active site, this negative charge will be stabilized by the positively charged, doubly protonated, histidine of the catalytic triad. Such transition state stabilization is not possible in case of the CNN motif, providing a rationale for the absence of the CNN triad in the thiolase superfamily.

CONCLUDING REMARKS

Our kinetic data highlight the importance of oxyanion hole I for Claisen condensation catalyzed by thiolases, and the structural data indicate mutually stabilizing interactions between the side chains of Asn316 and His348. The structural data also highlight that small changes of the hydrogen bond donors in oxyanion hole I affect the precise active site hydrogen bonding geometry. This is sufficient for a large effect on the catalytic proficiency of the condensation reaction. In some cases, also the detailed mode of binding of the substrate is affected, as is the case for CoA in the H348A active site. The hydrogen bonding scheme

of the active site in the absence and presence of acetyl-CoA is likely to be different for the Cys378−Wat49 interaction. In the presence of acetyl-CoA the deprotonated Cys378 is favored, as is also required for the condensation reaction (clockwise reaction 5 in Figure 1B). This notion highlights the importance of Wat49 for the reactivity of Cys378, whereas Wat82 is critically important for the condensation catalysis. Our studies confirm that oxyanion hole I in biosynthetic thiolase is critical for transition state stabilization in the condensation reaction, but not for binding the substrate.

ACKNOWLEDGMENT

We appreciate very much the help of Dr. Pirilä with the biophysical characterizations. We thank Drs. Banaszak and Barycki for providing the plasmid of the dehydrogenase linker enzyme and Drs. Pihko, Haapalainen, and Lambeir for many stimulating discussions. We also thank the staff of the ESRF beamlines ID-14-1 and ID-14-2 for their expert support. We thank very much Drs. Ulrich Bergmann and Antti Haapalainen for help with the mass spectrometry experiments.

REFERENCES

1. Walsh, C. T. (1979) Enzymatic Reaction Mechanisms , W.H. Freeman and Company, San Francisco, CA.
2. Heath, R. J., and Rock, C. O. (2002) The Claisen condensation in biology. *Nat. Prod. Rep. 19*, 581–596.
3. Austin, M. B., and Noel, J. P. (2003) The chalcone synthase superfamily of type III polyketide synthases. *Nat. Prod. Rep. 20*, 79–110.
4. Jiang, C., Kim, S. Y., and Suh, D.-Y. (2008) Divergent evolution of the thiolase superfamily and chalcone synthase family. *Mol. Phylogen. Evol. 49*, 691–701.
5. Peretó, J., López-Garcia, P., and Moreira, D. (2005) Phylogenetic analysis of eukaryotic thiolases suggests multiple proteobacterial origins. *J. Mol. Evol. 61*, 65–74.
6. Williams, S. F., Palmer, M. A., Peoples, O. P., Walsh, C. T., Sinskey, A. J., and Masamune, S. (1992) Biosynthetic thiolase from *Zoogloea ramigera*. Mutagenesis of the putative active-site base Cys-378 to Ser-378 changes the partitioning of the acetyl S-enzyme intermediate. *J. Biol. Chem. 267*, 16041–16043.
7. Kursula, P., Ojala, J., Lambeir, A.-M., and Wierenga, R. K. (2002) The catalytic cycle of biosynthetic thiolase: A conformational journey of an acetyl group through four binding modes and two oxyanion holes. *Biochemistry 41*, 15543–15556.
8. Haapalainen, A. M., Meriläinen, G., and Wierenga, R. K. (2006) The thiolase superfamily: condensing enzymes with diverse reaction specificities. *Trends Biochem. Sci. 31*, 64–71.
9. Crabtree, K., McCoy, E., Boyle, W. C., and Rohlich, G. A. (1965) Isolation, identification, and metabolic role of the sudanophilic granules of *Zoogloea ramigera*. *Appl. Microbiol. 13*, 218–226.
10. Stevenson, L. H., and Socolofsky, M. D. (1966) Cyst formation and poly-β-hydroxybutyric acid accumulation in *Azotobacter*. *J. Bacteriol. 91*, 304–310.
11. White, S. W., Zheng, J., Zhang, Y. M., and Rock (2005) The structural biology of type II fatty acid biosynthesis. *Annu. Rev. Biochem. 74*, 791–831.
12. Modis, Y., and Wierenga, R. K. (2000) Crystallographic analysis of the reaction pathway of *Zoogloea ramigera* biosynthetic thiolase. *J. Mol. Biol. 297*, 1171–1182.
13. Blow, D. (2000) So do we understand how enzymes work? *Structure 8*, R77–81.
14. Frey, P. A., Hegeman, A. D. (2007) Enzymatic Reaction Mechanisms, Oxford University Press, New York.
15. Silman, I., and Sussman, J. L. (2008) Acetylcholinesterase: How is structure related to function? *Chem. Biol. Interact. 175*, 3–10.
16. Nicolas, A., Egmond, M., Verrips, C. T., de Vlieg, J., Longhi, S., Cambillau, C., and Martinez, C. (1996) Contribution of cutinase serine 42 side chain to the stabilization of the oxyanion transition state. *Biochemistry 35*, 398–410.
17. Wells, J. A., Cunningham, B. C., Graycar, T. P., and Estell, D. A. (1986) Importance of hydrogen bond formation in stabilizing the transition state of subtilisin. *Phil Trans. R. Soc., A 317*, 415–413.
18. Ménard, R., Carrière, J., Laflamme, P., Plouffe, C., Khouri, H. E., Vernet, T., Tessier, D. C., Thomas, D. Y., and Storer, A. C. (1991) Contribution of the glutamine 19 side chain to transition-state stabilization in the oxyanion hole of papain. *Biochemistry 30*, 8924–8928.
19. Magnusson, A., Hult, K., and Holmquist, M. (2001) Creation of an enantioselective hydrolase by engineered substrate-assisted catalysis. *J. Am. Chem. Soc. 123*, 4354–4355.
20. Fersht, A. R., Shi, J. P., Knill-Jones, J., Lowe, D. M., Wilkinson, A. J., Blow, D. M., Brick, P., Carter, P., Waye, M. M., and Winter, G. (1985) Hydrogen bonding and biological specificity analysed by protein engineering. *Nature 314*, 235–238.
21. Fersht, A. R. (1999) Structure and Mechanism in Protein Science . W. H. Freeman and Company, New York.
22. Pihko, P., Rapakko, S., Wierenga, R. K. (2009) Oxyanion holes and their mimics, in Hydrogen Bonding in Organic Synthesis (Pihko, P., Ed.), Wiley-VCH Verlag, Weinheim, Germany, pp 43–71.
23. Evans, C. T., Kurz, L. C., Remington, S. J., and Srere, P. A. (1996) Active site mutants of pig citrate synthase: effects of mutations on the enzyme catalytic and structural properties. *Biochemistry. 35*, 10661–10672.
24. Hamed, R. B., Batchelar, E. T., Clifton, I. J., and Schofield, C. J. (2008) Mechanisms and structures of crotonase superfamily enzymes—how nature controls enolate and oxyanion reactivity. *Cell. Mol. Life Sci. 65*, 2507–2527.
25. Sigala, P. A., Kraut, D. A., Caaveiro, J. M., Pybus, B., Ruben, E. A., Ringe, D., Petsko, G. A., and Herschlag, D. (2008) Testing geometrical discrimination within an enzyme active site: constrained hydrogen bonding in the ketosteroid isomerase oxyanion hole. *J. Am. Chem. Soc. 130*, 13696–13708.
26. Modis, Y., and Wierenga, R. K. (1999) A biosynthetic thiolase in complex with a reaction intermediate: the crystal structure provides new insights into the catalytic mechanism. *Structure 7*, 1279–1290.
27. Barycki, J. J., O'Brien, L. K., Strauss, A. W., and Banaszak, L. J. (2000) Sequestration of the active by interdomain shifting: crystallographic and spectroscopic evidence for distinct conformations of L-3-hydroxyacyl-CoA dehydrogenase. *J. Biol. Chem. 275*, 27186–27196.
28. Barycki, J. J., O'Brien, L. K., Bratt, J. M., Zhang, R., Sanishvili, R., Strauss, A. W., and Banaszak, L. J. (1999) Biochemical characterization and crystal structure determination of human heart short chain L-3-hydroxyacyl-CoA dehydrogenase provide insights into catalytic mechanism. *Biochemistry 38*, 5786–5798.
29. Middleton, B. (1973) The oxoacyl-CoA thiolases of animal tissues. *Biochem. J. 132*, 717–730.
30. Haapalainen, A. M., Meriläinen, G., Pirilä, P. L., Kondo, N., Fukao, T., and Wierenga, R. K. (2007) Crystallographic and kinetic studies of human mitochondrial acetoacetyl-CoA thiolase: the importance of potassium and chloride ions for its structure and function. *Biochemistry 46*, 4305–4321.
31. Kabsch, W. (1993) Automatic processing of rotation diffraction data from crystals of initially unknown symmetry and cell constants. *J. Appl. Crystallogr. 26*, 795–800.
32. Leslie, A. G. W. (1992) Recent changes to the MOSFLM package for processing film and image plate data. Joint CCP4+ ESF-EAMCB Newsletter on Protein Crystallography 26.
33. Evans, P. (2006) Scaling and assessment of data quality. *Acta Crystallogr., Sect. D: Biol. Crystallogr. 62*, 72–82.
34. McCoy, A. J., Grosse-Kunstleve, R. W., Adams, P. D., Winn, M. D., Storoni, L. C., and Read, R. J. (2007) Phaser crystallographic software. *J. Appl. Crystallogr. 40*, 658–674.
35. Vagin, A., and Teplyakov, A. (1997) MOLREP: an automated program for molecular replacement. *J. Appl. Crystallogr. 30*, 1022–1025.
36. Collaborative Computational Project, Number 4. (1994) The CCP4 suite: programs for protein crystallography. Acta Crystallogr., Sect. D: Biol. Crystallogr. 50, 760−763.
37. Murshudov, G. N., Vagin, A. A., and Dodson, E. J. (1997) Refinement of macromolecular structures by the maximum-likelihood method. *Acta Crystallogr., Sect. D: Biol. Crystallogr. 53*, 240–255.
38. Emsley, P., and Cowtan, K. (2004) Coot: model building tools for molecular graphics. *Acta Crystallogr., Sect. D: Biol. Crystallogr. 60*, 2126–2132.
39. Adams, P. D., Grosse-Kunstleve, R. W., Hung, L.-W., Ioerger, T. R., McCoy, A. J., Moriarty, N. W., Read, R. J., Sacchettini, J. C., Sauter, N. K., and Terwilliger, T. C. (2002) PHENIX: building new software for automated crystallographic structure determination. *Acta Crystallogr., Sect. D: Biol. Crystallogr. 58*, 1948–1954.
40. Riddles, P. W., Blakeley, R. L., Zerner, B., and Fong, J. C. (1983) Reassessment of Ellman's reagent. *Methods Enzymol. 91*, 49–60.

41. Thompson, S., Mayerl, F., Peoples, O. P., Masamune, S., Sinskey, A. J., and Walsh, C. T. (1989) Mechanistic studies on beta-ketoacyl thiolase from *Zoogloea ramigera*: identification of the active-site nucleophile as Cys89, its mutation to Ser89, and kinetic and thermodynamic characterization of wild-type and mutant enzymes. *Biochemistry 28*, 5735–5742.
42. Meriläinen, G., Schmitz, W., Wierenga, R. K., and Kursula, P. (2008) The sulfur atoms of the substrate CoA and the catalytic cysteine are required for a productive mode of substrate binding in bacterial biosynthetic thiolase, a thioester-dependent enzyme. *FEBS J. 275*, 6136–6148.
43. Krissinel, E., and Henrick, K. (2004) Secondary structure matching (SSM), a new tool for fast protein structure alignment in three dimensions. *Acta Crystallogr., Sect. D: Biol. Crystallogr. 60*, 2256–2268.
44. Masamune, S., Walsh, C. T., Sinskey, A. J., and Peoples, O. P. (1989) Poly-*R*-3-hydroxybutyrate (PHB) biosynthesis: mechanistic studies on the biological Claisen condensation catalysed by β-ketoacyl thiolase. *Pure Appl. Chem. 61*, 303–312.
45. Shan, S. O., and Herschlag, D. (1999) Hydrogen bonding in enzymatic catalysis: analysis of energetic contributions. *Methods Enzymol. 308*, 246–276.
46. Zeng, J., and Li, D. (2004) Expression and purification of His-tagged rat mitochondrial 3-ketoacyl-CoA thiolase wild-type and His 352 mutant proteins. *Prot. Expression Purif. 35*, 320–326.
47. Willadsen, P., and Eggerer, H. (1975) Substrate stereochemistry of the acetyl-CoA acetyltransferase reaction. *Eur. J. Biochem. 54*, 253–258.
48. Davis, J. T., Moore, R. N., Imperiali, B., Pratt, A. J., Kobayashi, K., Masamune, S., Sinskey, A. J., Walsh, C. T., Fukui, T., and Tomita, K. (1987) Biosynthetic thiolase from *Zoogloea ramigera*. I. Preliminary characterization and analysis of proton transfer reaction. *J. Biol. Chem. 262*, 82–89.
49. Amyes, T. L., and Richard, J. P. (1992) Generation and stability of a simple thiol ester enolate in aqueous solution. *J. Am. Chem. Soc. 114*, 10297–10302.
50. Kursula, P., Sikkila, H., Fukao, T., Kondo, N., and Wierenga, R. K. (2005) High resolution crystal structures of human cytosolic thiolase (CT). A comparison of the active sites of human CT, bacterial thiolase, and bacterial KAS I. *J. Mol. Biol. 347*, 189–201.
51. Palmer, M. A., Differding, E., Gamboni, R., Williams, S. F., Peoples, O. P., Walsh, C. T., Sinskey, A. J., and Masamune, S. (1991) Biosynthetic thiolase from *Zoogloea ramigera*. Evidence for a mechanism involving Cys-378 as the active site base. *J. Biol. Chem. 266*, 8369–8375.
52. Eggerer, H. (1965) Zum Mechanismus der Biologischen Umwandlung von Citronensäure. IV. Citrate synthase ist eine Acetyl-CoA-Enolase. *Biochem. Z. 343*, 111–138.
53. Bell, A. F., Wu, J., Feng, Y., and Tonge, P. J. (2001) Involvement of glycine 141 in substrate activation by enoyl-CoA hydratase. *Biochemistry 40*, 1725–1733.
54. Ishikawa, M., Tsuchiya, D., Oyama, T., Tsunaka, Y., and Morikawa, K. (2004) Structural basis for channelling mechanism of a fatty acid beta-oxidation multienzyme complex. *EMBO J. 23*, 2745–2754.
55. Mathieu, M., Modis, Y., Zeelen, J. P., Engel, C. K., Abagyan, R. A., Ahlberg, A., Rasmussen, B., Lamzin, V. S., Kunau, W. H., and Wierenga, R. K. (1997) The 1.8 A crystal structure of the dimeric peroxisomal 3-ketoacyl-CoA thiolase of *Saccharomyces cerevisiae*: implications for substrate binding and reaction mechanism. *J. Mol. Biol. 273*, 714–728.
56. Sundaramoorthy, R., Micossi, E., Alphey, M. S., Germain, V., Bryce, J. H., Smith, S. M., Leonard, G. A., and Hunter, W. N. (2006) The crystal structure of a plant 3-ketoacyl-CoA thiolase reveals the potential for redox control of peroxisomal fatty acid beta-oxidation. *J. Mol. Biol. 359*, 347–357.
57. Lovell, S. C., Davis, I. W., Arendall, W. B., III, de Bakker, P. I., Word, J. M., Prisant, M. G., Richardson, J. S., and Richardson, D. C. (2003) Structure validation by Cα geometry: φ, ψ and Cβ deviation. *Proteins 50*, 437–450.